VarRCWA: An Adaptive High-Order Rigorous Coupled Wave Analysis Method

Ziwei Zhu[1] and Changxi Zheng[*1]

[1]Department of Computer Science, Columbia University, New York, New York 10027, USA

February 1, 2022

Abstract

Semi-analytical methods, such as rigorous coupled wave analysis, have been pivotal for numerical analysis of photonic structures. In comparison to other methods, they offer much faster computation, especially for structures with constant cross-sectional shapes (such as metasurface units). However, when the cross-sectional shape varies even mildly (such as a taper), existing semi-analytical methods suffer from high computational cost. We show that the existing methods can be viewed as a zeroth-order approximation with respect to the structure's cross-sectional variation. We instead derive a high-order perturbative expansion with respect to the cross-sectional variation. Based on this expansion, we propose a new semi-analytical method that is fast to compute even in presence of large cross-sectional shape variation. Furthermore, we design an algorithm that automatically discretizes the structure in a way that achieves a user specified accuracy level while at the same time reducing the computational cost.

1 Introduction

Numerical simulation is a fundamental tool for understanding photonic structures. Among many popular methods, semi-analytical methods, such as rigorous coupled wave analysis (RCWA) [15], have been widely used for analyzing such devices as metasurfaces [6], gratings [14] and waveguides [24]. In comparison to other methods, such as finite-difference time-domain (FDTD) methods, semi-analytical methods often have much lower computational cost.

This advantage stems from how semi-analytical methods discretize Maxwell's equations. In contrast to other approaches (e.g., FDTD methods) that discretize the spatial domain fully (i.e., in all three dimensions) [23], semi-analytical methods discretize the spatial domain partially (e.g., in only x- and y-dimension but not z-dimension). This is possible because many photonic structures have a primary light propagation direction (referred in this paper as z-direction; see Fig. 2). In some cases, along the light propagation direction, the structure's cross-sectional shape stays unchanged (e.g., a metasurface unit). Therefore, we do not have to discretize the structure along z-direction; instead, light propagation in the structure can be viewed as superposition of individual propagating modes experiencing phase shifts. This is the fundamental view that enables semi-analytical methods to reduce computational cost (see **2.1**).
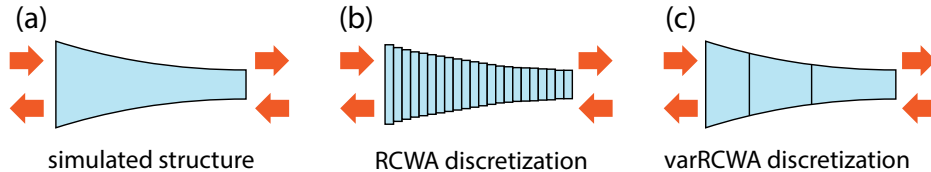
---

[*]cxz@cs.columbia.edu

1

Figure 1: **Discretization in conventional and our method.** Provided a photonic structure with varying cross-sectional shape (a), conventional semi-analytical methods (such as RCWA) must discretize the structure along the wave propagation direction into many thin sections (b), leading to expensive computation. (c) Our method discretizes the structure adaptively into a much smaller number of sections, thanks to the use of higher-order perturbative expansions. The arrows indicate the incoming and outgoing direction of light waves.

However, this view becomes unsound for many photonic structures wherein along the primary light propagation direction, the structure's cross section varies [13, 17]. A common example is photonic waveguides (such as a taper; see Fig. 1-a). To simulate these photonic structures using semi-analytical methods, one has to further discretize the structure along z-direction into a series of thin sections [9, 11] (see Fig. 1-b). In each section, the cross-sectional shape is assumed unchanged, and thereby a semi-analytical method can be used to simulate that section. Yet, this approach requires a large number of sections, which in turn devastate the computational advantage of semi-analytical methods. Apart from the computational cost, it is often unclear how many discrete sections are needed to achieve certain accuracy. In practice, one has to rely on trail and error to choose a proper resolution for sufficient accuracy. Oftentimes, to obtain satisfactory results, multiple runs of the simulation method (each with a different resolution) are needed.

In this work, we overcome these limitations. Our method requires no trial and error, thus much easier to use: provided a photonic structure and a user-specified accuracy level (i.e., a real number), our method automatically decides how to discretize the structure in z-direction, aiming to reduce the overall computational cost while achieving the desired accuracy. To obtain simulation results of user-specified accuracy, only one run is needed.

To this end, our core development is twofold: 1) We show that the conventional semi-analytical methods (such as RCWA) are merely zeroth-order approximation with respect to the structure's cross-sectional variation. Through a novel change of variable, we propose a high-order semi-analytical method, which allows the structure's cross section to vary over z-direction, without discretizing it into thin sections. 2) Leveraging this high-order method, we introduce an algorithm that automatically and adaptively discretizes the structure to achieve a user specified accuracy level. For regions where the cross section varies rapidly in z-direction, our algorithm will slice the structure in fine resolution to ensure simulation accuracy; for regions with little cross-sectional variance, it will discretize them coarsely to save computational cost.

We use our method to analyze various photonic structures, and compare it with conventional semi-analytical methods (such as RCWA). We show that our method, as a higher-order approach, indeed converges faster. As a result, to obtain the same level of accuracy, our method requires much less computational time and no resolution tuning at all.

2 Method

We now present our core development. To understand the rationale behind our development, we start by briefly reviewing the limitations of widely used semi-analytical methods.

2.1 Established Semi-analytical Methods and Their Limitations

Semi-analytical methods discretize the spatial domain of Maxwell's equations in x- and y-directions but not in z-direction. In frequency domain, Maxwell's equations become into

$$\frac{\partial \boldsymbol{e}}{\partial z} = \frac{j}{k_0} \boldsymbol{P} \boldsymbol{h} \quad \text{and} \quad \frac{\partial \boldsymbol{h}}{\partial z} = \frac{j}{k_0} \boldsymbol{Q} \boldsymbol{e}, \tag{1}$$

where the vectors $\boldsymbol{e}$ and $\boldsymbol{h}$ are discrete representations of the electric and magnetic fields on an xy-plane at a z position, and the matrices $\boldsymbol{P}$ and $\boldsymbol{Q}$ encode the distributions of material permeability and permittivity on the xy-plane at the same z position. Depending on specific representations of $\boldsymbol{e}$ and $\boldsymbol{h}$, different semi-analytical methods emerge. The most widely used (e.g., for the analysis of metasurfaces [6], gratings [14] and waveguides [24]) is rigorous coupled wave analysis (RCWA) method, wherein $\boldsymbol{e}$ and $\boldsymbol{h}$ are discretized using 2D Fourier basis on the xy-plane. In this paper, our development can be applied to semi-analytical methods in general (such as the method of lines [18]), although our implementation and numerical experiments focus in particular on the RCWA method.

When the structure's cross-sectional shape is fixed along z-direction, both $\boldsymbol{P}$ and $\boldsymbol{Q}$ in (1) are constant matrices, and Eq. (1) can be solved through an eigenvalue decomposition, that is, $\boldsymbol{P}\boldsymbol{Q} = \boldsymbol{W}\boldsymbol{\Lambda}^2\boldsymbol{W}^{-1}$. The resulting $\boldsymbol{W}$ and $\boldsymbol{\Lambda}$ allow us to express the solution of (1) as

$$\boldsymbol{e} = \frac{1}{2}\boldsymbol{W}\left(e^{\boldsymbol{\Lambda} z}\boldsymbol{a}_L + e^{-\boldsymbol{\Lambda} z}\boldsymbol{b}_L\right) \quad \text{and} \quad \boldsymbol{h} = \frac{1}{2}\boldsymbol{V}\left(e^{\boldsymbol{\Lambda} z}\boldsymbol{a}_L - e^{-\boldsymbol{\Lambda} z}\boldsymbol{b}_L\right). \tag{2}$$

Here $\boldsymbol{V}$ is the basis for describing the cross-sectional magnetic field, related to the eigenvectors $\boldsymbol{W}$ (i.e., the basis for electric field) through $\boldsymbol{V} = \boldsymbol{Q}\boldsymbol{W}\boldsymbol{\Lambda}^{-1}$; $\boldsymbol{a}_\mathrm{L}$ and $\boldsymbol{b}_\mathrm{L}$ are vectors stacking the coefficients of the forward and backward light waves at the left end of the structure (see Fig. 2). In addition, from Eq. (2), we can define the structure's *scattering matrix*, which relates the output state of an optical wave after propagating through the structure with its input state, namely

$$\begin{bmatrix} \boldsymbol{a}_\mathrm{R} \\ \boldsymbol{b}_\mathrm{L} \end{bmatrix} = \boldsymbol{S} \begin{bmatrix} \boldsymbol{a}_\mathrm{L} \\ \boldsymbol{b}_\mathrm{R} \end{bmatrix}, \quad \text{where} \quad \boldsymbol{S} = \begin{bmatrix} \boldsymbol{T}_\mathrm{LR} & \boldsymbol{R}_\mathrm{R} \\ \boldsymbol{R}_\mathrm{L} & \boldsymbol{T}_\mathrm{RL} \end{bmatrix}, \tag{3}$$

where, corresponding to $\boldsymbol{a}_\mathrm{L}$ and $\boldsymbol{b}_\mathrm{L}$, $\boldsymbol{a}_\mathrm{R}$ and $\boldsymbol{b}_\mathrm{R}$ describe the forward and backward waves at the right end (see Fig. 2). Once the scattering matrix is known, the structure's optical performance (e.g., mode conversion efficiency and phase shift of a waveguide) can be directly computed.

When the structure's cross-sectional shape varies along z-direction, one has to split the structure into a series of small sections so that every section can be approximated as having a fixed cross section (Fig. 1-b). Each section i is then analyzed through the aforementioned process, from which one can compute its scattering matrix $\boldsymbol{S}_i$. Finally, by combining all the scattering matrices using Redheffer star product [19], the entire structure's scattering matrix is obtained.

Limitations. In semi-analytical methods, the assumption of having a fixed cross section can be viewed as a zeroth-order approximation of the structure (as derived in Sec. 2.2). To achieve sufficient accuracy, such a crude approximation must be remedied with small structure length. As a result, even mild cross-sectional variation requires a large number of discrete sections (Fig. 1-b). For every section, an eigenvalue decomposition is needed, and thus its computational cost
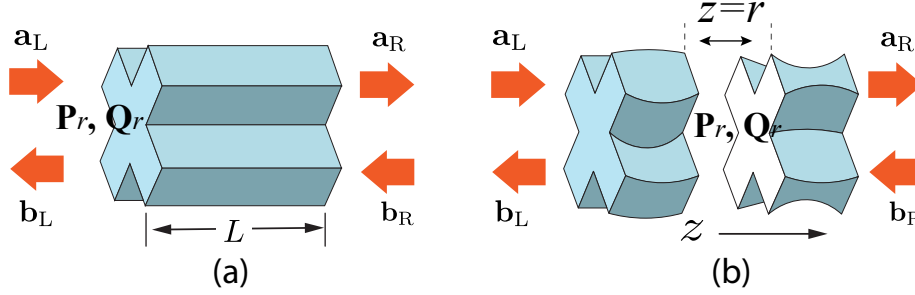
Figure 2: **Notation.** Provided a photonic structure section, we model light wave propagation in four components: the incoming and outgoing waves at both the left and right ends, as shown by the orange arrows. (a) A section with constant cross-sectional shape has fixed material matrices $\boldsymbol{P}_r$ and $\boldsymbol{Q}_r$. (b) When a section has a varying cross-sectional shape, we choose a specific position $z = r$ (called reference position), and use the material matrices, $\boldsymbol{P}_r$ and $\boldsymbol{Q}_r$, at $z = r$ to construct the basis for describing forward and backward waves. Our method treats such a section as a perturbation of a section with constant cross-sectional shape in (a), and leverages a perturbative expansion for numerical simulation. Here for visualization purpose, we cut through the section at $z = r$ to reveal the cross-section at $z = r$, which may differ from the cross-sectional shape at its two ends.

is further scaled by the total number of sections. To reduce the computational cost, we need to reduce the total number of discrete sections (Fig. 1-c) while retaining simulation accuracy. This motivates us to seek a high-order semi-analytical method, one that accounts for the cross-sectional variation in a long section and thereby reduces the total number of sections.

2.2   High-order Semi-analytical Methods

Consider a section of photonic structure along z-direction. Suppose its cross-sectional shape varies, that is, in Eq. (1), $\boldsymbol{P}$ and $\boldsymbol{Q}$ are not constant matrices; they change over z. In this case, the solution of (1) is not as simple as (2). Now, our goal is to express the solution of (1) as a perturbative expansion with respect to cross-section variation (Fig. 2), and this expansion will serve as the core numerical recipe of our method.

Naïve solution.   To understand the insight of our development, we start with a naïve (but impractical) expansion form of the solution. First, inspired by Eq. (2), we use a set of basis vectors $\boldsymbol{W}$ and $\boldsymbol{V}$ to describe cross-sectional electric and magnetic fields respectively—the specific choice of $\boldsymbol{W}$ and $\boldsymbol{V}$ in presence of varying cross section will be described shortly. The cross-sectional electric and magnetic fields, $\boldsymbol{e}$ and $\boldsymbol{h}$, are formed by light waves propagating forward and backward in the structure, with the relations:

$$\boldsymbol{a}(z) = \boldsymbol{W}^{-1}\boldsymbol{e}(z) + \boldsymbol{V}^{-1}\boldsymbol{h}(z) \ \text{ and } \ \boldsymbol{b}(z) = \boldsymbol{W}^{-1}\boldsymbol{e}(z) - \boldsymbol{V}^{-1}\boldsymbol{h}(z), \tag{4}$$

where $\boldsymbol{a}$ and $\boldsymbol{b}$ are coefficients in the chosen basis for describing the forward and backward waves, respectively, and they vary over z. Next, to establish a differential equation of $\boldsymbol{a}$ (and $\boldsymbol{b}$), we differentiate both sides of (4), and then using Maxwell's equations (1), we obtain

$$\frac{\partial \boldsymbol{a}}{\partial z} = \boldsymbol{W}^{-1}\frac{\partial \boldsymbol{e}}{\partial z} + \boldsymbol{V}^{-1}\frac{\partial \boldsymbol{h}}{\partial z} = \frac{j}{2k_0}\left[\boldsymbol{W}^{-1}\boldsymbol{P}\boldsymbol{V}\left(\boldsymbol{a} - \boldsymbol{b}\right) + \boldsymbol{V}^{-1}\boldsymbol{Q}\boldsymbol{W}\left(\boldsymbol{a} + \boldsymbol{b}\right)\right]. \tag{5}$$

4

Equivalently, we have the integral equation

$$\boldsymbol{a}(z) = \boldsymbol{a}(z_L) + \frac{j}{2k_0} \int_{z_L}^{z} \left[\left(\boldsymbol{W}^{-1}\boldsymbol{P}\boldsymbol{V} + \boldsymbol{V}^{-1}\boldsymbol{Q}\boldsymbol{W} \right) \boldsymbol{a}(z') + \left(\boldsymbol{V}^{-1}\boldsymbol{Q}\boldsymbol{W} - \boldsymbol{W}^{-1}\boldsymbol{P}\boldsymbol{V} \right) \boldsymbol{b}(z') \right] \mathrm{d}z', \quad (6)$$

where z_L is the starting z position of the considered structure section. Note also that both $\boldsymbol{P}$ and $\boldsymbol{Q}$ vary over z, and a similar integral equation can be obtained for $\boldsymbol{b}(z)$. Equation (6), in theory, allows us to express $\boldsymbol{a}(z)$ as a perturbative expansion. This is achieved by recursively substituting $\boldsymbol{a}(z')$ in the integrand with Eq. (6) itself up to a certain order (and similarly for $\boldsymbol{b}(z)$). For example, to obtain a first-order expansion, one can replace $\boldsymbol{a}(z')$ and $\boldsymbol{b}(z')$ in (6) with their zeroth-order approximations $\boldsymbol{a}_L \approx \boldsymbol{a}(z_L)$ and $\boldsymbol{b}_R \approx \boldsymbol{b}(z_R)$.

To use this expansion for analyzing a long section (and thereby reduce the total number of sections), the norms of $\boldsymbol{W}^{-1}\boldsymbol{P}\boldsymbol{V}$ and $\boldsymbol{V}^{-1}\boldsymbol{Q}\boldsymbol{W}$ must be sufficiently small—an intuitive explanation of this requirement is provided in Supplement 1. This requirement, however, is hardly satisfied in practice, as both $\boldsymbol{P}$ and $\boldsymbol{Q}$ depend on the cross-sectional material distribution, and their norms may become arbitrarily large. Nevertheless, the development of this expansion motivates a viable strategy: in order to obtain a stable perturbative expansion, we need to avoid using $\boldsymbol{P}$ and $\boldsymbol{Q}$ in an integral equation like (6); instead, we seek an expansion that involves only the variation of $\boldsymbol{P}$ and $\boldsymbol{Q}$ over z.

Preconditioned solution. Our proposed expansion starts with a change of variables. We introduce two variables:

$$\tilde{\boldsymbol{a}} = e^{-\frac{j}{k_0}\boldsymbol{\Lambda}z}\boldsymbol{a} \quad \text{and} \quad \tilde{\boldsymbol{b}} = e^{\frac{j}{k_0}\boldsymbol{\Lambda}z}\boldsymbol{b}, \tag{7}$$

where $\boldsymbol{\Lambda}$ is the eigenvalue matrix resulted from eigen-decomposition $\boldsymbol{P}_r\boldsymbol{Q}_r = \boldsymbol{W}\boldsymbol{\Lambda}^2\boldsymbol{W}^{-1}$. Here, $\boldsymbol{P}_r$ and $\boldsymbol{Q}_r$ are fixed matrices encoding the distribution of material permeability and permittivity at a particular $z = r$ position. Ideally, the cross section at $z = r$ is chosen to represent the "average" cross section over the entire section so that it can be used to construct the basis vectors $\boldsymbol{W}$ and $\boldsymbol{V}$. We therefore refer to this position as the *reference position* of the section (see Fig. 2-b). While in theory one can choose any r position, in practice we simply use the mid-point of the section. The resulting $\boldsymbol{W}$ (and $\boldsymbol{V}$ through $\boldsymbol{V} = \boldsymbol{Q}\boldsymbol{W}\boldsymbol{\Lambda}^{-1}$) is used as the basis for describing forward and backward waves (recall Eq. (4)).

This change of variables is the key to introduce the variation of $\boldsymbol{P}$ and $\boldsymbol{Q}$ in an integral equation similar to (6). By differentiating (7) and using Eq. (1), we obtain the following differential equations (see the derivation in Supplement 2):

$$\frac{\partial \tilde{\boldsymbol{a}}}{\partial z} = \frac{j}{2k_0} e^{\left(-\frac{j}{k_0}\boldsymbol{\Lambda}z\right)} \delta\boldsymbol{A} e^{\left(\frac{j}{k_0}\boldsymbol{\Lambda}z\right)} \tilde{\boldsymbol{a}} - \frac{j}{2k_0} e^{\left(-\frac{j}{k_0}\boldsymbol{\Lambda}z\right)} \delta\boldsymbol{B} e^{\left(-\frac{j}{k_0}\boldsymbol{\Lambda}z\right)} \tilde{\boldsymbol{b}},$$
$$\frac{\partial \tilde{\boldsymbol{b}}}{\partial z} = \frac{j}{2k_0} e^{\left(\frac{j}{k_0}\boldsymbol{\Lambda}z\right)} \delta\boldsymbol{B} e^{\left(\frac{j}{k_0}\boldsymbol{\Lambda}z\right)} \tilde{\boldsymbol{a}} - \frac{j}{2k_0} e^{\left(\frac{j}{k_0}\boldsymbol{\Lambda}z\right)} \delta\boldsymbol{A} e^{\left(-\frac{j}{k_0}\boldsymbol{\Lambda}z\right)} \tilde{\boldsymbol{b}}, \tag{8}$$

where $\delta\boldsymbol{A}$ and $\delta\boldsymbol{B}$ are related to the material variation along z-direction, namely,

$$\delta\boldsymbol{A}(z) = \boldsymbol{W}^{-1}\left(\boldsymbol{P}(z) - \boldsymbol{P}_r\right)\boldsymbol{V} + \boldsymbol{V}^{-1}\left(\boldsymbol{Q}(z) - \boldsymbol{Q}_r\right)\boldsymbol{W},$$
$$\delta\boldsymbol{B}(z) = \boldsymbol{W}^{-1}\left(\boldsymbol{P}(z) - \boldsymbol{P}_r\right)\boldsymbol{V} - \boldsymbol{V}^{-1}\left(\boldsymbol{Q}(z) - \boldsymbol{Q}_r\right)\boldsymbol{W}. \tag{9}$$

Next, we rewrite Eq. (8) in integral forms and replace $\tilde{\boldsymbol{a}}$ and $\tilde{\boldsymbol{b}}$ using Eq. (7). This leads to a

5

new set of integral equations of $\boldsymbol{a}(z)$ and $\boldsymbol{b}(z)$, ones that differ from (6):

$$\boldsymbol{a}(z) = e^{\frac{j}{k_0}\boldsymbol{\Lambda}(z-z_L)}\boldsymbol{a}_L + \frac{j}{2k_0}\int_{z_L}^z e^{\frac{j}{k_0}\boldsymbol{\Lambda}(z-z')}\delta\boldsymbol{A}(z')\boldsymbol{a}(z')\mathrm{d}z' - \frac{j}{2k_0}\int_{z_L}^z e^{\frac{j}{k_0}\boldsymbol{\Lambda}(z-z')}\delta\boldsymbol{B}(z')\boldsymbol{b}(z')\mathrm{d}z'$$

$$(10)$$

$$\boldsymbol{b}(z) = e^{\frac{j}{k_0}\boldsymbol{\Lambda}(z_R-z)}\boldsymbol{b}_R - \frac{j}{2k_0}\int_z^{z_R} e^{\frac{j}{k_0}\boldsymbol{\Lambda}(z'-z)}\delta\boldsymbol{B}(z')\boldsymbol{a}(z')\mathrm{d}z' + \frac{j}{2k_0}\int_z^{z_R} e^{\frac{j}{k_0}\boldsymbol{\Lambda}(z'-z)}\delta\boldsymbol{A}(z')\boldsymbol{b}(z')\mathrm{d}z'.$$

$$(11)$$

Note that here the two equations are integrated from different directions. In Eq. (10), we use $\boldsymbol{a}_L$ at the left end of the section as the initial value, and the integral is along the forward direction. On the contrary, Eq. (11) integrates along the backward direction, using $\boldsymbol{b}_R$ as the initial value. In this way, all the propagation phase terms (i.e., $e^{j\boldsymbol{\Lambda}\Delta z/k_0}$) become smaller than one, and thereby the numerical computation of these integrals stays stable.

Now, we can construct perturbative expansions of the outgoing waves $\boldsymbol{a}_R$ and $\boldsymbol{b}_L$. Similar to the construction of the naïve expansions above, we substitute $\boldsymbol{a}(z')$ and $\boldsymbol{b}(z')$ in the integral terms with Eqs. (10) and (11) themselves, and this substitution is done recursively up to a certain order. These expansions offer a numerical recipe for analyzing how the structure interacts with propagating waves. For example, provided the input waves to the section, including the forward wave at the left end (described by $\boldsymbol{a}_L$; see Fig. 2) and the backward wave at the right end (described by $\boldsymbol{b}_R$), the outgoing waves at the right and left ends can be estimated using the following first-order expansions:

$$\boldsymbol{a}_R \approx e^{\frac{j}{k_0}\boldsymbol{\Lambda}(z_R-z_L)}\boldsymbol{a}_L + \frac{j}{2k_0}\int_{z_L}^{z_R} e^{\frac{j}{k_0}\boldsymbol{\Lambda}(z_R-z')}\delta\boldsymbol{A}(z')e^{\frac{j}{k_0}\boldsymbol{\Lambda}(z'-z_L)}\mathrm{d}z'\boldsymbol{a}_L$$

$$- \frac{j}{2k_0}\int_{z_L}^{z_R} e^{\frac{j}{k_0}\boldsymbol{\Lambda}(z_R-z')}\delta\boldsymbol{B}(z')e^{\frac{j}{k_0}\boldsymbol{\Lambda}(z_R-z')}\mathrm{d}z'\boldsymbol{b}_R,$$

$$(12)$$

$$\boldsymbol{b}_L \approx e^{\frac{j}{k_0}\boldsymbol{\Lambda}(z_R-z_L)}\boldsymbol{b}_R + \frac{j}{2k_0}\int_{z_L}^{z_R} e^{\frac{j}{k_0}\boldsymbol{\Lambda}(z'-z_L)}\delta\boldsymbol{A}(z')e^{\frac{j}{k_0}\boldsymbol{\Lambda}(z_R-z')}\mathrm{d}z'\boldsymbol{b}_R$$

$$- \frac{j}{2k_0}\int_{z_L}^{z_R} e^{\frac{j}{k_0}\boldsymbol{\Lambda}(z'-z_L)}\delta\boldsymbol{B}(z')e^{\frac{j}{k_0}\boldsymbol{\Lambda}(z'-z_L)}\mathrm{d}z'\boldsymbol{a}_L.$$

$$(13)$$

Remarkably, these expansions do not involve $\boldsymbol{W}^{-1}\boldsymbol{PV}$ or $\boldsymbol{V}^{-1}\boldsymbol{QW}$ (unlike (6)). But rather, their integrands depend on $\delta\boldsymbol{A}$ and $\delta\boldsymbol{B}$. Thus, Eqs. (12) and (13) can be viewed as a (first-order) perturbation solution of the outgoing waves. If the cross section is invariant, $\delta\boldsymbol{A} = \delta\boldsymbol{B} = \boldsymbol{0}$, and the integral terms in Eqs. (12) and (13) vanish. In this case, the expressions are precisely the same as the conventional semi-analytical methods, indicating that the conventional semi-analytical methods are zeroth-order perturbation in presence of cross-sectional variation. If the cross section is slowly varying over z, the norms of $\delta\boldsymbol{A}$ and $\delta\boldsymbol{B}$ are small, and thereby the first-order perturbation converges even for a long section. This contrasts starkly to the naïve expansions based on Eq. (6), whose reliance on $\boldsymbol{P}$ and $\boldsymbol{Q}$ drastically restricts the section length. If the cross section varies quickly, the norms of $\delta\boldsymbol{A}$ and $\delta\boldsymbol{B}$ may be large, and we have to use short section length to ensure convergence of our perturbation solution.

Discussion: alternative approaches. Maxwell's equation (1) may also be viewed as an initial value problem provided with the electric and magnetic fields at $z = z_L$. Solution to this initial value problem can be expressed as a product integral that involves matrix exponentials [7, 21]:

$$\begin{bmatrix} \boldsymbol{e}(z_R) \\ \boldsymbol{h}(z_R) \end{bmatrix} = \lim_{N\to\infty}\prod_{i=N}^1 \exp\left(\frac{j(z_i - z_{i-1})}{k_0}\begin{bmatrix} \boldsymbol{0} & \boldsymbol{P}_r(z_{i-1}\to z_i) \\ \boldsymbol{Q}(z_{i-1}\to z_i) & \boldsymbol{0} \end{bmatrix}\right)\begin{bmatrix} \boldsymbol{e}(z_L) \\ \boldsymbol{h}(z_L) \end{bmatrix}. \quad (14)$$

In this expression, the structure is also discretized into a series of sections at z_i, where $z_L = z_0 < z_1 < \cdots < z_N = z_R$; and $\boldsymbol{P}_r$ and $\boldsymbol{Q}_r$ are permeability and permittivity matrices evaluated at the reference position of each section.

Numerical evaluation of (14), however, is rather challenging. Prior works use a low-order Taylor expansion of the matrix exponentials to evaluate (14) [10, 20]. But to use this expansion, section length must be excessively short (i.e., $z_i - z_{i-1} \leq 0.1\lambda$ where λ is the wavelength), and a large number of sections are needed.

Another approach is to convert the product of matrix exponential into the exponential of matrix summation, similar to $\prod \exp(x_i) = \exp(\sum_i x_i)$ for scalar values x_i. However, this is not straightforward because matrix multiplication is noncommutative. As a result, Magnus expansion [1, 2, 8] and Fer expansion [22] have been used to correct the use of exponential of matrix summation. In this vein, RCWA can be viewed as an approximation of Magnus expansion, as shown in [4]. Although a high-order approximation of Magnus expansion was introduced in [4], it still requires each discrete section to be short even with small cross-sectional variation.

A more fundamental problem of this line of approaches stems from the treatment of initial value problem. Light propagating in photonic structures almost always scatters, resulting in forward and backward propagations. But treating it as an initial value problem implies that only a single direction is considered, thus causing the numerical integration unstable. It is this reason that our method, like conventional RCWA, separates the light waves into forward and backward going components, and integrate them along two separate directions (recall (10) and (11)).

2.3 Numerical Implementation with Adaptive Discretization

Numerical integration. The integrals in Eqs. (12) and (13) can be numerically evaluated using a quadrature rule. In practice, we use the quadrature rule that samples three positions, at z_L, $\frac{z_L + z_R}{2}$, and z_R, respectively, and the integral is estimated by weighted summation of the integrand values at the sampled positions. This quadrature rule involves only matrix multiplications, and thus can be computed at low cost; in practice, we implement it on a Graphics Processing Unit (GPU). Consequently, the major cost of evaluating wave propagation in a single section (using (12) and (13)) comes from the eigen-decomposition that computes $\boldsymbol{W}$, $\boldsymbol{\Lambda}$, and $\boldsymbol{V}$ at the reference position. For a single structure section, the eigen-decomposition is also needed in conventional semi-analytical methods. Our perturbative expansion is more accurate at a trivial cost of the additional numerical integration. But when it comes to simulating an entire photonic structure, our expansion enables adaptively discretization of the structure along z-direction, thereby reducing the overall computational cost and outperforming the conventional methods. Next, we describe our algorithm for simulating an entire structure.

Adaptive discretization. We now consider the simulation of an entire photonic structure, not just a single section. We propose an algorithm that adaptively discretizes the structure in z-direction and simulates wave propagation. Input to our algorithm is a photonic structure and a desired accuracy level (i.e., a real number). The goal here is to achieve the desired accuracy while reducing the overall computational cost.

Our proposed algorithm is outlined in Algorithm 1. The key idea behind this algorithm is as follows: starting from the entire structure as a single section, it recursively subdivides a structure section into M subsections (Line 5 in Algorithm 1). The subdivision occurs when an estimated simulation error of the current section is larger than the user specified accuracy level α (Line 2 in Algorithm 1). Afterwards, all subsections are simulated individually, and they may be subdivided further in a recursive way (Line 9). For each subsection, we compute how the

---

Algorithm 1: Adaptive-Variant-RCWA($z_{\min}$, $z_{\max}$, α)

    Input: Simulated region along z axis: $[z_{\min}, z_{\max}]$, error bound α
    Output: Scattering matrix from $z_{\min}$ to $z_{\max}$
    Data: Simulated Geometry $\mathcal{G}$

1 Evaluate high order scattering matrix S according to Supplement 3 by sampling on $\mathcal{G}$
2 **if** *estimated error (see Supplement 6)* $< \alpha$ **then**
3 | **return** S
4 **else**
5 | Subdivide this section into M subsections (z_0, z_1), (z_1, z_2), ..., (z_{M-1}, z_M)
6 | where $z_{\min} = z_0 < z_1 < \cdots < z_M = z_{\max}$
7 | Find a reference point for each subsection.
8 | **for** $i = 1, ..., M$ **do**
9 | | scattering matrix $S_i(z_{i-1} \to z_i) \leftarrow$ Adaptive-Variant-RCWA(z_{i-1}, z_i, α)
10 | | Project the basis of S_i to match the basis of S_{i-1} (see Supplement 4)
11 | **return** $S \leftarrow$ Redheffer star product of $S_1, ..., S_M$.

---

wave propagates using (12) and (13), and further compute this subsection's scattering matrix (Line 1; see Supplement 3 for detailed formulas). Lastly, the scattering matrices of individual subsections are combined through Redheffer star product [19] to form the scattering matrix of the parent section (Line 11).

We estimate the error by computing the discrepancy of asymptotic expansions in two consecutive orders (e.g., between zeroth order and first order) Supplement 6—such an error estimation has been used in other asymptotic expansions [3, 5]. In practice, when a section is subdivided, we subdivide it into three subsections (i.e., $M = 3$). In this way, the eigen-decomposition needed for the parent section can be reused for simulating the central subsection (see Fig. 3-b). An alternative is to use binary subdivision (i.e., $M = 2$), which we will compare in our numerical experiments in **3.2**.

Through recursive subdivision, adaptive discretization on z-direction naturally emerges: regions with rapidly varying cross-sections will be more subdivided, and thereby the algorithm automatically uses fine sections to ensure accuracy; meanwhile, in smoothly varying regions, it uses low resolution to save computation.

3   Results

We conduct numerical experiments to validate the accuracy of our method and compare its performance with conventional semi-analytical methods. Since there are different ways of implementing semi-analytical methods (depending on how $\boldsymbol{e}$ and $\boldsymbol{h}$ in (1) are represented), we adopt the most widely used representation, the RCWA method [15].

We implement both our method and the conventional RCWA in C++ programming language. Numerical computation in both methods, such as matrix multiplication and eigen-decomposition, can benefit from parallel computation. We therefore leverage CUDA [16] on Nvidia Graphics Processing Units (GPUs) to accelerate the computation in both methods.
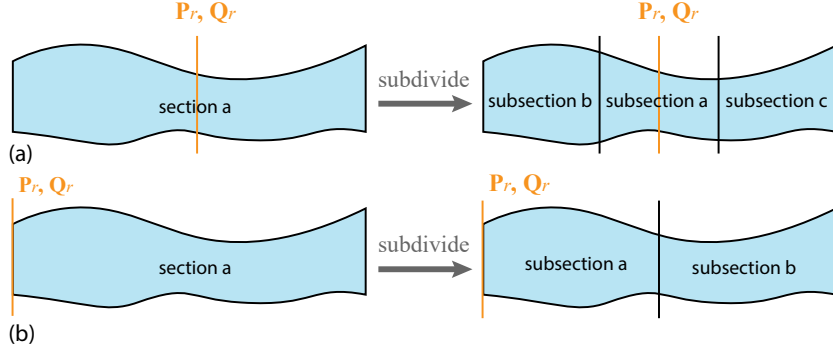
Figure 3: (a) we choose the midpoint of each section as its reference point to evaluate $\boldsymbol{P}_r$ and $\boldsymbol{Q}_r$. When subdividing one section, we subdivide it evenly into three subsections. In this way, the midpoint of the mid-section is the same as that of the parent section, and thus $\boldsymbol{P}_r$ and $\boldsymbol{Q}_r$ can be reused. (b) We also experimented with subdividing a section evenly into two subsections (i.e., $M = 2$). This strategy is proper when we use the endpoint of a section as its reference point.
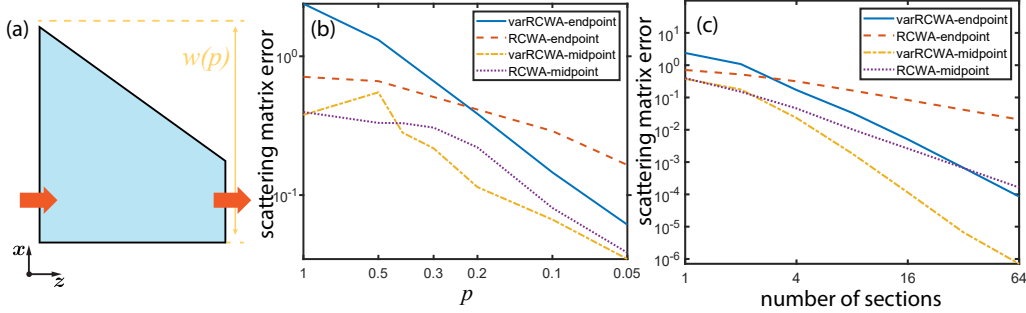

Figure 4: (a) We use VarRCWA to analyze a waveguide whose cross-sectional shape changes linearly. The length of the waveguide is 1 μm. Its width on the right end is fixed at 2.6 μm, and we use a parameter p to specify the width on the left end. When $p = 1$, the left width is 3.7 μm, and when $p = 0$, the left width is the same as the right end (i.e., 2.6 μm). (b) We simulate this waveguide with no z-direction discretization (i.e., treating it as a single section), and measure the scattering matrix errors as p changes. (c) We then increase the z-direction resolution, and measure the scattering matrix errors as p changes. In the legends, "midpoint" indicates the use of the middle position as the reference position to construct $\boldsymbol{P}_r$ and $\boldsymbol{Q}_r$(see Fig. 3-a), and "endpoint" indicates the use of the end position of a section as the reference position (see Fig. 3-b). See **Data File 1-2** for underlying values.

3.1 Validation

To validate the accuracy of our method, we consider a trapezoid-shaped waveguide as shown in Fig. 4-a. This waveguide has a fixed 220nm thickness, and we use a parameter p to control its cross-sectional variation from its left to right end (see Fig. 4 caption).

First, we verify that our method has higher accuracy than the conventional method. To evaluate the accuracy, we first discretize the waveguide into 256 sections, and compute the entire waveguide's scattering matrix $\boldsymbol{S}^*$ using the conventional RCWA. This $\boldsymbol{S}^*$ is then used as a

9

ground-truth to measure a max norm error, $\|\boldsymbol{S} - \boldsymbol{S}^*\|_{\max}$, where $\boldsymbol{S}$ is the scattering matrix resulted from either our method or the conventional RCWA. In both cases, we use a single section to simulate the entire waveguide for fair comparison. We measure the errors while the cross-sectional variation (controlled by p) changes. As shown in Fig. 4-b, when the cross-sectional variation is large (i.e., $p \to 1$), our method is more accurate than conventional RCWA, thanks to its higher-order approximation. When the variation becomes small (i.e., $p \to 0$), both methods have comparable accuracy.

Further, we evaluate the convergence of our method. We again consider the waveguide shown in Fig. 4 (with $p = 1$), and evaluate the scattering matrix errors of our method and the conventional RCWA while the z-direction resolutions (in both methods) increases. The results are reported in Fig. 4-c: our method converges faster; as the resolution becomes higher, our method is much more accurate.

3.2   Performance for Various Waveguides

Next, we test the performance of our method for analyzing various photonic structures. The shapes of these structures are described in Fig. 5. For each structure, the ground-truth scattering matrix is computed using the conventional RCWA with a high resolution in z-direction ($N = 1024$). Provided the ground-truth scattering matrix, we measure the performance-accuracy curve for our method and the conventional RCWA: for our method, we progressively reduce the error threshold (i.e., α in Algorithm 1); and for each error threshold, we measure the resulting scattering matrix error and the computational cost. This allows us to plot a curve showing how the accuracy changes over the computation time. Similary, for conventional RCWA, we progressively increase the z-direction resolution, and measure the scattering matrix error and computation time. All the timings are measured on a workstation with 8 Intel Xeon(R) E5-1620 CPUs running at 3.60GHz and an NVIDIA GeForce GTX 1080 GPU.

The resulting performance-accuracy curves are shown in Fig. 5. Given a fixed accuracy level (indicated by the green horizontal line in Fig. 5), our method is significantly faster. For example, to compute the scattering matrix with an error around 10^{-4}, out method is at least $3.5\times$ faster than the conventional RCWA for all test cases. In certain cases such as Fig. 5-e, our method is even an order of magnitude faster. In all cases, our method converges faster than the conventional RCWA, confirming that ours is a higher-order method. This means that as the speedup of our method will become more pronounced as the desired accuracy level increases.

We also note that when the conventional RCWA is used for analyzing a particular photonic structure, there exists no guideline to determine the z-direction resolution for a certain accuracy level. As a result, in practice, one has to rely on multiple trials to choose a proper resolution, and thus spend more time than what is reported in Fig. 5.

Finally, we evaluate our method on two real-world examples shown in Fig. 6, namely a Y-shaped waveguide and a frequency splitter. The former is smoothed out from our design of 90/10 splitter [25] using Bézier curve and the latter is reported in [12]. Again, the ground-truth scattering matrices for both cases are obtained by the conventional RCWA, with 8192 discrete sections for the Y-shaped waveguide and 32768 sections for the frequency splitter, since the latter has more complex geometry. As shown in Fig. 6, our method converges faster, and for sufficiently high accuracy, our method has much lower computational cost.

4   Conclusion

In summary, we present a high-order semi-analytical method. Our method is best suited for simulating photonic structures whose cross-sectional shapes vary along the propagation direction.
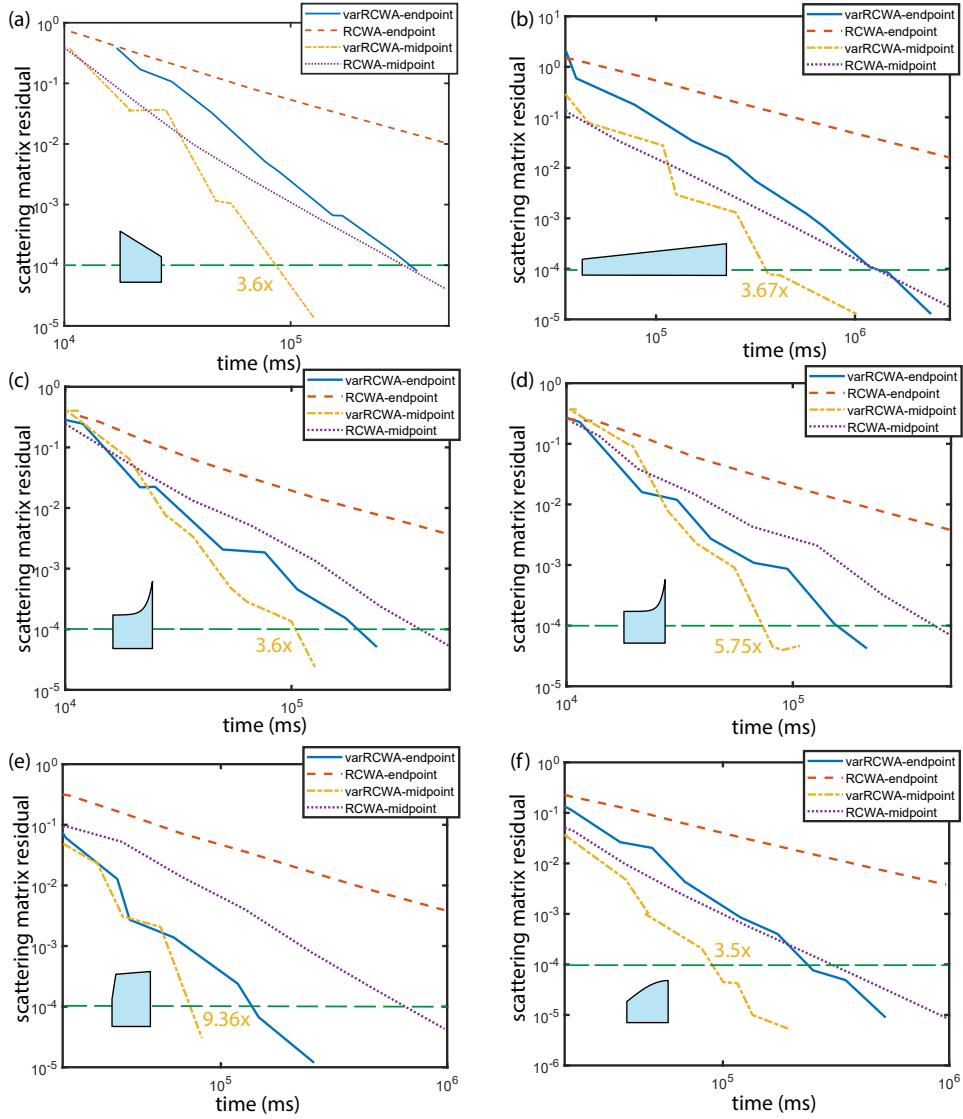
Figure 5: **Tests on various waveguide geometries.** (a) a trapezoid waveguide. (b) a long waveguide of 10μm length. (c-d) waveguides with exponential shape changes along one side. (e) a piecewise-linear waveguide. (f) a waveguide with a sinusoidal side variation. All waveguides except (b) are of length 1μm. Their thicknesses are fixed at 0.22μm. The speedup of our method over the conventional RCWA for the same accuracy level (i.e., 10^{-4}) is marked in yellow color. See **Data File 3-8** for underlying values.
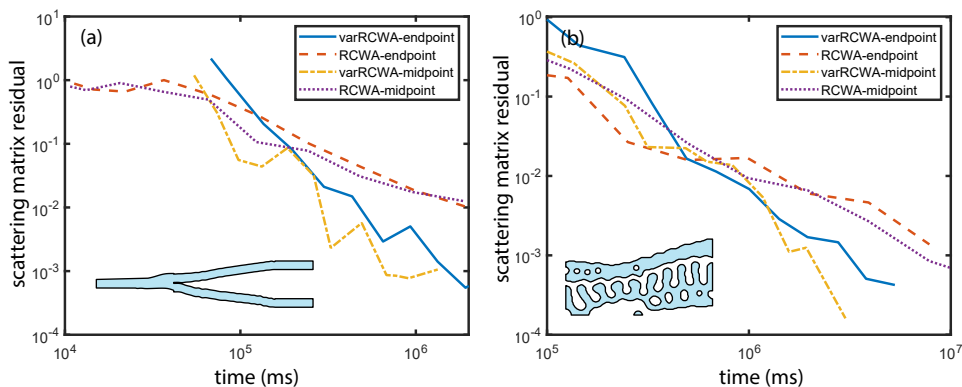
Figure 6: **Tests on complex photonic structures.** (a) a Y-shape waveguide. (b) a frequency splitter reported in [12]. See **Data File 9-12** for underlying values.

In comparison to conventional semi-analytical methods, our method is faster and more accurate. In addition, our method allows the user to specify an accuracy level, and adaptively discretizes the structure along z-direction to achieve the desired accuracy.

In future, this work can be extended in various directions. Currently, when subdivision of a section occurs, the section is subdivided into three subsections uniformly. It is also possible to subdivide non-uniformly, according to the local cross-sectional shape of the structure. Moreover, our implementation uses the first-order expansion that we derived, although we can easily extend it to use even higher order expansion by recursively substituting a lower-order expansion into (10) and (11). In practice, our method based on the first-order expansion already outperforms the conventional RCWA.

Disclosures. The authors declare no conflicts of interest.

See Supplement 1 for supporting content.

References

[1] BLANES, S., CASAS, F., OTEO, J., AND ROS, J. Magnus and fer expansions for matrix differential equations: the convergence problem. *Journal of Physics A: Mathematical and General 31*, 1 (1998), 259.

[2] BLANES, S., CASAS, F., OTEO, J.-A., AND ROS, J. The magnus expansion and some of its applications. *Physics reports 470*, 5-6 (2009), 151–238.

[3] CHEN, X., ZHENG, C., XU, W., AND ZHOU, K. An asymptotic numerical method for inverse elastic shape design. *ACM Transactions on Graphics (Proceedings of SIGGRAPH 2014) 33*, 4 (Aug. 2014).

[4] CHU, H. Finite difference approach to optical scattering of gratings. In *Advanced Characterization Techniques for Optics, Semiconductors, and Nanotechnologies* (2003), vol. 5188, International Society for Optics and Photonics, pp. 358–370.

[5] COCHELIN, B. A path-following technique via an asymptotic-numerical method. *Computers & structures 53*, 5 (1994), 1181–1192.

[6] DIVITT, S., ZHU, W., ZHANG, C., LEZEC, H. J., AND AGRAWAL, A. Ultrafast optical pulse shaping using dielectric metasurfaces. *Science 364*, 6443 (2019), 890–894.

[7] HELTON, J., AND STUCKWISCH, S. Numerical approximation of product integrals. *Journal of Mathematical Analysis and Applications 56*, 2 (1976), 410–437.

[8] ISERLES, A., AND NØRSETT, S. P. On the solution of linear differential equations in lie groups. *Philosophical Transactions of the Royal Society of London. Series A: Mathematical, Physical and Engineering Sciences 357*, 1754 (1999), 983–1019.

[9] JING, X., JIN, S., TIAN, Y., LIANG, P., DONG, Q., AND WANG, L. Analysis of the sinusoidal nanopatterning grating structure. *Optics & Laser Technology 48* (2013), 160–166.

[10] LI, J., SHI, L. H., MA, Y., RAN, Y., LIU, Y., AND WANG, J. Efficient and stable implementation of rcwa for ultrathin multilayer gratings: T-matrix approach without solving eigenvalues. *IEEE Antennas and Wireless Propagation Letters* (2020).

[11] LIU, V., AND FAN, S. S4: A free electromagnetic solver for layered periodic structures. *Computer Physics Communications 183*, 10 (2012), 2233–2244.

[12] LUMERICAL. GDS pattern extraction for inverse designed devices using contours method, 2021.

[13] MILLER, S. A., CHANG, Y.-C., PHARE, C. T., SHIN, M. C., ZADKA, M., ROBERTS, S. P., STERN, B., JI, X., MOHANTY, A., GORDILLO, O. A. J., ET AL. Large-scale optical phased array using a low-power multi-pass silicon photonic platform. *Optica 7*, 1 (2020), 3–6.

[14] MOHAMAD, H., ESSAIDI, S., BLAIZE, S., MACIAS, D., BENECH, P., AND MORAND, A. Fast fourier factorization for differential method and rcwa: a powerful tool for the modeling of non-lamellar metallic diffraction gratings. *Optical and Quantum Electronics 52*, 2 (2020), 1–13.

[15] MOHARAM, M., AND GAYLORD, T. Rigorous coupled-wave analysis of planar-grating diffraction. *JOSA 71*, 7 (1981), 811–818.

[16] NVIDIA, VINGELMANN, P., AND FITZEK, F. H. Cuda, release: 10.2.89, 2020.

[17] PIGGOTT, A. Y., LU, J., LAGOUDAKIS, K. G., PETYKIEWICZ, J., BABINEC, T. M., AND VUČKOVIĆ, J. Inverse design and demonstration of a compact and broadband on-chip wavelength demultiplexer. *Nature Photonics 9*, 6 (2015), 374–377.

[18] PREGLA, R., AND PASCHER, W. The method of lines. *Numerical techniques for microwave and millimeter wave passive structures 1* (1989), 381–446.

[19] REDHEFFER, R. Inequalities for a matrix riccati equation. *Journal of Mathematics and Mechanics* (1959), 349–367.

[20] ROBERTS, C. M., AND PODOLSKIY, V. A. Rigorous diffraction interface theory. *Applied Physics Letters 110*, 17 (2017), 171108.

[21] SLAVÍK, A. *Product integration, its history and applications.* Matfyzpress Prague, 2007.

[22] TAKEGOSHI, K., MIYAZAWA, N., SHARMA, K., AND MADHU, P. Comparison among magnus/floquet/fer expansion schemes in solid-state nmr. *The Journal of chemical physics 142*, 13 (2015), 134201.

[23] YEE, K. Numerical solution of initial boundary value problems involving maxwell's equations in isotropic media. *IEEE Transactions on antennas and propagation 14*, 3 (1966), 302–307.

[24] ZHU, Z., DAVE, U. D., LIPSON, M., AND ZHENG, C. Inverse geometric design of fabrication-robust nanophotonic waveguides. In *2020 Conference on Lasers and Electro-Optics (CLEO)* (2020), IEEE, pp. 1–2.

[25] ZHU, Z., DAVE, U. D., LIPSON, M., AND ZHENG, C. Ultra-broadband nanophotonics via adaptive inverse design. In *2021 Conference on Lasers and Electro-Optics (CLEO)* (2021), IEEE, pp. 1–2.

VarRCWA: An Adaptive High-Order Rigorous Coupled Wave Analysis Method: supplemental document

February 1, 2022

1 Explanation of the requirement of the integrand in Eqn. (6)

To use Eqn. (6) for a long section, the coefficients $\boldsymbol{W}^{-1}\boldsymbol{PV}$ and $\boldsymbol{V}^{-1}\boldsymbol{QW}$ should be small enough. We explain the intuition behind this requirement using a simple example, a scalar differential equation in a similar form of Eqn. (5)

$$\frac{\mathrm{d}}{\mathrm{d}z}y(z) = ay(z), \tag{1}$$

where a is a constant, similar to $\boldsymbol{W}^{-1}\boldsymbol{PV}$ and $\boldsymbol{V}^{-1}\boldsymbol{QW}$ in Eqn. (5), and $y(z)$ is similar to the vectors $\boldsymbol{a}(z')$ and $\boldsymbol{b}(z')$ therein. This equation can be written as an integral form similar to Eqn. (6):

$$y(z) = y(z_L) + \int_{z_L}^{z} ay(z')\mathrm{d}z'. \tag{2}$$

By recursively substituting (2) into $y(z')$, we get

$$y(z) = \left[1 + \int a\mathrm{d}z' + \frac{1}{2}\left(\int a\mathrm{d}z'\right)^2 + \cdots\right] y(z_L), \tag{3}$$

where the right-hand side is a Taylor expansion of $\exp\left(\int a\mathrm{d}z'\right)$:

$$\exp\left(\int a\mathrm{d}z'\right) = 1 + \int a\mathrm{d}z' + \frac{1}{2}\left(\int a\mathrm{d}z'\right)^2 + \cdots \tag{4}$$

Although Taylor expansion of an exponential always converges for all $\int a\mathrm{d}z'$, if we truncate this series to the first order, the residual, which is

$$\mathrm{Re} = \left|\exp\left(\int a\mathrm{d}z'\right) - 1 - \int a\mathrm{d}z'\right| = \left|\left(\int a\mathrm{d}z'\right)^2\right|\left|\frac{1}{2} + o\left(\int a\mathrm{d}z'\right)\right|, \tag{5}$$

1

scales with the magnitude of $\int a dz' = a(z - z_L) = aL$. In order to increase the length L of this integral while maintaining the same integral value aL (hence the accuracy), a should be small enough. Similarly $\boldsymbol{W}^{-1}\boldsymbol{P}\boldsymbol{V}$ and $\boldsymbol{V}^{-1}\boldsymbol{Q}\boldsymbol{W}$ should be small enough to ensure plausible accuracy of the first order truncation. $\boldsymbol{W}$ and $\boldsymbol{V}$ do not scale with the section length as they are eigenvectors. Therefore, $\boldsymbol{P}$ and $\boldsymbol{Q}$ must have small enough norms, which unfortunately can not be guaranteed.

2 Derivation of Eqn. (8)

Note that the coefficients $\boldsymbol{P}$ and $\boldsymbol{Q}$, which depend on the cross-sectional material distribution, can be arbitrarily large, even if the section has a fixed cross section. We therefore wish to replace them by $\delta\boldsymbol{P}$ and $\delta\boldsymbol{Q}$, which depend only on the cross-sectional variation of the section. To this end, instead of differentiating $\boldsymbol{a}$ and $\boldsymbol{b}$, we scale $\boldsymbol{a}$ and $\boldsymbol{b}$ first in order to cancel out some terms and construct $\delta\boldsymbol{P}$ and $\delta\boldsymbol{Q}$. In particular, let

$$\tilde{\boldsymbol{a}} = \gamma_1(z)\boldsymbol{a}(z) \tag{6}$$

$$\tilde{\boldsymbol{b}} = \gamma_2(z)\boldsymbol{b}(z) \tag{7}$$

for some specific choices of $\gamma_1(z)$ and $\gamma_2(z)$. Inspired by [1] and the derivation of RCWA, after several trials, we find $\gamma_1(z)$ and $\gamma_2(z)$ in Eqs. (7).

Firstly, we differentiate $\tilde{\boldsymbol{a}}$ in the first part of Eqn. (7) as

$$\frac{\partial\tilde{\boldsymbol{a}}}{\partial z} = -\frac{j}{k_0}\boldsymbol{\Lambda}\tilde{\boldsymbol{a}} + \exp\left(-\frac{j}{k_0}\boldsymbol{\Lambda}z\right)\frac{\partial\boldsymbol{a}}{\partial z}. \tag{8}$$

The first term $-\frac{j}{k_0}\boldsymbol{\Lambda}\tilde{\boldsymbol{a}}$ is emerged to construct $\delta\boldsymbol{P}$ and $\delta\boldsymbol{Q}$. Now substitude Eqs. (5) in (8):

$$\frac{\partial\tilde{\boldsymbol{a}}}{\partial z} = \frac{j}{2k_0}\exp\left(-\frac{j}{k_0}\boldsymbol{\Lambda}z\right)\left(-2\boldsymbol{\Lambda}\boldsymbol{a} + \boldsymbol{W}^{-1}\boldsymbol{P}\boldsymbol{V}\left(\boldsymbol{a} - \boldsymbol{b}\right) + \boldsymbol{V}^{-1}\boldsymbol{Q}\boldsymbol{W}\left(\boldsymbol{a} + \boldsymbol{b}\right)\right). \tag{9}$$

From $\boldsymbol{P}_r\boldsymbol{Q}_r = \boldsymbol{W}\boldsymbol{\Lambda}^2\boldsymbol{W}^{-1}$ and $\boldsymbol{V} = \boldsymbol{Q}_r\boldsymbol{W}\boldsymbol{\Lambda}^{-1}$, we get the following relations:

$$\boldsymbol{\Lambda} = \boldsymbol{V}^{-1}\boldsymbol{Q}_r\boldsymbol{W} = \boldsymbol{W}^{-1}\boldsymbol{P}_r\boldsymbol{V}. \tag{10}$$

Next, by substituting Eqs. (10) into (9), we obtain

$$\frac{\partial\tilde{\boldsymbol{a}}}{\partial z} = \frac{j}{2k_0}\exp\left(-\frac{j}{k_0}\boldsymbol{\Lambda}z\right)\left(\boldsymbol{W}^{-1}\left(\boldsymbol{P} - \boldsymbol{P}_r\right)\boldsymbol{V}\boldsymbol{a} + \boldsymbol{V}^{-1}\left(\boldsymbol{Q} - \boldsymbol{Q}_r\right)\boldsymbol{W}\boldsymbol{a} - \boldsymbol{W}^{-1}\boldsymbol{P}\boldsymbol{V}\boldsymbol{b} + \boldsymbol{V}^{-1}\boldsymbol{Q}\boldsymbol{W}\boldsymbol{b}\right)$$

$$= \frac{j}{2k_0}\exp\left(-\frac{j}{k_0}\boldsymbol{\Lambda}z\right)\left(\boldsymbol{W}^{-1}\delta\boldsymbol{P}\boldsymbol{V}\boldsymbol{a} + \boldsymbol{V}^{-1}\delta\boldsymbol{Q}\boldsymbol{W}\boldsymbol{a} - \boldsymbol{W}^{-1}\boldsymbol{P}\boldsymbol{V}\boldsymbol{b} + \boldsymbol{V}^{-1}\boldsymbol{Q}\boldsymbol{W}\boldsymbol{b}\right)$$

There are still $\boldsymbol{P}$ and $\boldsymbol{Q}$ in the coefficients of $\boldsymbol{b}$. But the signs of the coefficients are different, one is positive and the other one is negative. Therefore, we can add an extra zero term

$(\boldsymbol{\Lambda} - \boldsymbol{\Lambda})\boldsymbol{b}$ to help with the cancellation:

$$
\begin{aligned}
\frac{\partial \tilde{\boldsymbol{a}}}{\partial z} &= \frac{j}{2k_0} \exp\left(-\frac{j}{k_0}\boldsymbol{\Lambda}z\right)\left(\delta\boldsymbol{A}\boldsymbol{a} - \boldsymbol{W}^{-1}\boldsymbol{P}\boldsymbol{V}\boldsymbol{b} + \boldsymbol{V}^{-1}\boldsymbol{Q}\boldsymbol{W}\boldsymbol{b} + (\boldsymbol{\Lambda}-\boldsymbol{\Lambda})\boldsymbol{b}\right) \\
&= \frac{j}{2k_0} \exp\left(-\frac{j}{k_0}\boldsymbol{\Lambda}z\right)\left(\delta\boldsymbol{A}\boldsymbol{a} - \boldsymbol{W}^{-1}\boldsymbol{P}\boldsymbol{V}\boldsymbol{b} + \boldsymbol{V}^{-1}\boldsymbol{Q}\boldsymbol{W}\boldsymbol{b} + \left(\boldsymbol{W}^{-1}\boldsymbol{P}_r\boldsymbol{V} - \boldsymbol{V}^{-1}\boldsymbol{Q}_r\boldsymbol{W}\right)\boldsymbol{b}\right) \\
&= \frac{j}{2k_0} \exp\left(-\frac{j}{k_0}\boldsymbol{\Lambda}z\right)\left(\delta\boldsymbol{A}\boldsymbol{a} - \delta\boldsymbol{B}\boldsymbol{b}\right) \\
&= \frac{j}{2k_0} \exp\left(-\frac{j}{k_0}\boldsymbol{\Lambda}z\right)\delta\boldsymbol{A}\exp\left(\frac{j}{k_0}\boldsymbol{\Lambda}z\right)\tilde{\boldsymbol{a}} - \frac{j}{2k_0}\exp\left(-\frac{j}{k_0}\boldsymbol{\Lambda}z\right)\delta\boldsymbol{B}\exp\left(-\frac{j}{k_0}\boldsymbol{\Lambda}z\right)\tilde{\boldsymbol{b}}.
\end{aligned}
\tag{11}
$$

Thanks to the symmetry of $\tilde{\boldsymbol{a}}$ and $\tilde{\boldsymbol{b}}$, we can get the differentiation of $\tilde{\boldsymbol{b}}$ the same way.

3 Construction of the high order scattering matrix

The matrix elements in Eqn.(3) can be extracted from Eqs. (12) and (13) as follows:

$$
\boldsymbol{T}_{LR} = e^{\frac{j}{k_0}\boldsymbol{\Lambda}(z_R - z_L)} + \frac{j}{2k_0}\int_{z_L}^{z_R} e^{\frac{j}{k_0}\boldsymbol{\Lambda}(z_R - z')}\delta\boldsymbol{A}(z')e^{\frac{j}{k_0}\boldsymbol{\Lambda}(z'-z_L)}\mathrm{d}z'
\tag{12}
$$

$$
\boldsymbol{R}_R = -\frac{j}{2k_0}\int_{z_L}^{z_R} e^{\frac{j}{k_0}\boldsymbol{\Lambda}(z_R - z')}\delta\boldsymbol{B}(z')e^{\frac{j}{k_0}\boldsymbol{\Lambda}(z_R - z')}\mathrm{d}z'
\tag{13}
$$

$$
\boldsymbol{R}_L = -\frac{j}{2k_0}\int_{z_L}^{z_R} e^{\frac{j}{k_0}\boldsymbol{\Lambda}(z' - z_L)}\delta\boldsymbol{B}(z')e^{\frac{j}{k_0}\boldsymbol{\Lambda}(z' - z_L)}\mathrm{d}z'
\tag{14}
$$

$$
\boldsymbol{T}_{RL} = e^{\frac{j}{k_0}\boldsymbol{\Lambda}(z_R - z_L)} + \frac{j}{2k_0}\int_{z_L}^{z_R} e^{\frac{j}{k_0}\boldsymbol{\Lambda}(z' - z_L)}\delta\boldsymbol{A}(z')e^{\frac{j}{k_0}\boldsymbol{\Lambda}(z_R - z')}\mathrm{d}z'.
\tag{15}
$$

4 Projection of scattering matrix

Because the scattering matrix at a section i in (given in Eqs. (23-26)) is expressed in the basis of eigenmodes at the reference position of section i. If the eigenmodes are different from those of section $(i-1)$, we need to reproject the scattering matrix at section i to match the eigenmodes of section $(i-1)$ before using Redheffer star product to multiply them together.

According to the continuity of the tangential fields at the interface between the two sections, if we denote the eigenmodes at section i as $\boldsymbol{W}_i$ and $\boldsymbol{V}_i$, and we use the superscript $(i-1)$ to denote the vector is represented in the basis of section $(i-1)$, while the vectors without superscripts are in the basis of the section i. From Eq. (2), we have

$$
\begin{aligned}
\boldsymbol{W}_{i-1}\left(\boldsymbol{a}_L^{(i-1)} + \boldsymbol{b}_L^{(i-1)}\right) &= \boldsymbol{W}_i\left(\boldsymbol{a}_L + \boldsymbol{b}_L\right) \\
\boldsymbol{V}_{i-1}\left(\boldsymbol{a}_L^{(i-1)} - \boldsymbol{b}_L^{(i-1)}\right) &= \boldsymbol{V}_i\left(\boldsymbol{a}_L - \boldsymbol{b}_L\right).
\end{aligned}
\tag{16}
$$

Now we denote

$$
\begin{aligned}
\boldsymbol{X} &= \frac{1}{2}\left(\boldsymbol{W}_i^{-1}\boldsymbol{W}_{i-1} + \boldsymbol{V}_i^{-1}\boldsymbol{V}_{i-1}\right) \\
\boldsymbol{Y} &= \frac{1}{2}\left(\boldsymbol{W}_i^{-1}\boldsymbol{W}_{i-1} - \boldsymbol{V}_i^{-1}\boldsymbol{V}_{i-1}\right),
\end{aligned}
\tag{17}
$$

which allow us to express $\boldsymbol{a}_L$ and $\boldsymbol{b}_L$ using (16), namely,

$$
\begin{aligned}
\boldsymbol{a}_L &= \boldsymbol{X}\boldsymbol{a}_L^{(i-1)} + \boldsymbol{Y}\boldsymbol{b}_L^{(i-1)} \\
\boldsymbol{b}_L &= \boldsymbol{Y}\boldsymbol{a}_L^{(i-1)} + \boldsymbol{X}\boldsymbol{b}_L^{(i-1)}.
\end{aligned}
\tag{18}
$$

Meanwhile, according to the scattering matrix definition in Eq. (3), we have

$$
\begin{aligned}
\boldsymbol{b}_L &= \boldsymbol{R}_L\boldsymbol{a}_L + \boldsymbol{T}_{RL}\boldsymbol{b}_R \\
(\boldsymbol{X} - \boldsymbol{R}_L\boldsymbol{Y})\,\boldsymbol{b}_L^{(i-1)} &= -\left(\boldsymbol{Y} - \boldsymbol{R}_L\boldsymbol{X}\right)\boldsymbol{a}_L^{(i-1)} + \boldsymbol{T}_{RL}\boldsymbol{b}_R.
\end{aligned}
\tag{19}
$$

By comparing (18) to (19), we obtain the recipe for reprojection of the scattering matrix:

$$
\begin{aligned}
\tilde{\boldsymbol{R}}_L &= -\left(\boldsymbol{X} - \boldsymbol{R}_L\boldsymbol{Y}\right)^{-1}\left(\boldsymbol{Y} - \boldsymbol{R}_L\boldsymbol{X}\right) \\
\tilde{\boldsymbol{T}}_{RL} &= \left(\boldsymbol{X} - \boldsymbol{R}_L\boldsymbol{Y}\right)^{-1}\boldsymbol{T}_{RL}.
\end{aligned}
\tag{20}
$$

Similarly, from

$$
\boldsymbol{a}_R = \boldsymbol{T}_{LR}\boldsymbol{X}\boldsymbol{a}_L^{(i-1)} + \boldsymbol{T}_{LR}\boldsymbol{Y}\left(\tilde{\boldsymbol{R}}_L\boldsymbol{a}_L^{(i-1)} + \tilde{\boldsymbol{T}}_{RL}\boldsymbol{b}_R\right) + \boldsymbol{R}_R\boldsymbol{b}_R,
\tag{21}
$$

We have

$$
\begin{aligned}
\tilde{\boldsymbol{T}}_{LR} &= \boldsymbol{T}_{LR}\boldsymbol{X} + \boldsymbol{T}_{LR}\boldsymbol{Y}\tilde{\boldsymbol{R}}_L \\
\tilde{\boldsymbol{R}}_R &= \boldsymbol{T}_{LR}\boldsymbol{Y}\tilde{\boldsymbol{T}}_{RL} + \boldsymbol{R}_R.
\end{aligned}
\tag{22}
$$

The projected scattering matrix elements $\tilde{\boldsymbol{R}}_L$, $\tilde{\boldsymbol{T}}_{RL}$, $\tilde{\boldsymbol{T}}_{LR}$, $\tilde{\boldsymbol{R}}_R$ can be left multiplied by the scattering matrix of section $(i-1)$.

5   CPU Implementation

We have also implemented our method on CPU. We choose the same structure as Fig. 5-a to run the experiments. As is shown in Fig 1, our method performs better no matter we choose the midpoint or endpoint as the reference point. However, because the program runs sequentially, the CPU implementation cannot parallelize the computation of matrix products, which is not so efficient. Therefore, matrix product still takes a noticeable amount of time (1/20 per operation) compared to eigenvalue decomposition. Although both RCWA and our method running on CPU are slower, our method is still faster compared to conventional RCWA, although the speedup of our method is not as significant as on GPU.
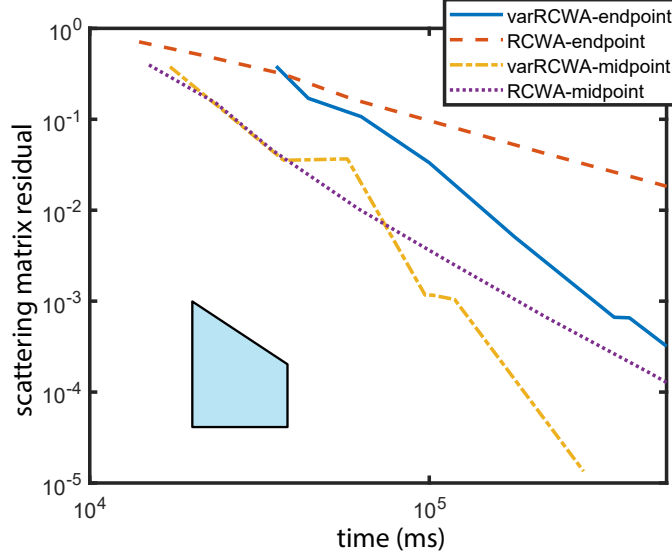
4

Figure 1: CPU implementation of the experiments in Fig. 5(a). See **Data File 13** for underlying values.

6   Error Estimation

When subdividing the waveguide, our algorithm checks if an estimated error meets the user-provided accuracy level α. To estimate the error, we compare the scattering matrix of the pth order and the $(p-1)$th order. In our case, we subtract the results standard RCWA $(p=0)$ from the results in Eqs. (23-26) $(p=1)$, and get the following four difference matrices

$$\Delta \boldsymbol{T}_{LR} = \frac{j}{2k_0} \int_{z_L}^{z_R} e^{\frac{j}{k_0}\boldsymbol{\Lambda}(z_R-z')} \delta \boldsymbol{A}(z') e^{\frac{j}{k_0}\boldsymbol{\Lambda}(z'-z_L)} \mathrm{d}z' \tag{23}$$

$$\Delta \boldsymbol{R}_{R} = -\frac{j}{2k_0} \int_{z_L}^{z_R} e^{\frac{j}{k_0}\boldsymbol{\Lambda}(z_R-z')} \delta \boldsymbol{B}(z') e^{\frac{j}{k_0}\boldsymbol{\Lambda}(z_R-z')} \mathrm{d}z' \tag{24}$$

$$\Delta \boldsymbol{R}_{L} = -\frac{j}{2k_0} \int_{z_L}^{z_R} e^{\frac{j}{k_0}\boldsymbol{\Lambda}(z'-z_L)} \delta \boldsymbol{B}(z') e^{\frac{j}{k_0}\boldsymbol{\Lambda}(z'-z_L)} \mathrm{d}z' \tag{25}$$

$$\Delta \boldsymbol{T}_{RL} = \frac{j}{2k_0} \int_{z_L}^{z_R} e^{\frac{j}{k_0}\boldsymbol{\Lambda}(z'-z_L)} \delta \boldsymbol{A}(z') e^{\frac{j}{k_0}\boldsymbol{\Lambda}(z_R-z')} \mathrm{d}z'. \tag{26}$$

We use the maximum value ε of the max norms of the above four matrices as the estimated error, and compare ε with user-provided α.

Although ε is estimated, any error caused by higher order perturbations should be smaller than ε. We have also compared this estimated error with the final error in the scattering

5

matrix for each experiments in Fig. 5. As is shown in Fig. 2, for each user-specified α, the real error is always smaller than α, which indicates it is a good overestimate.
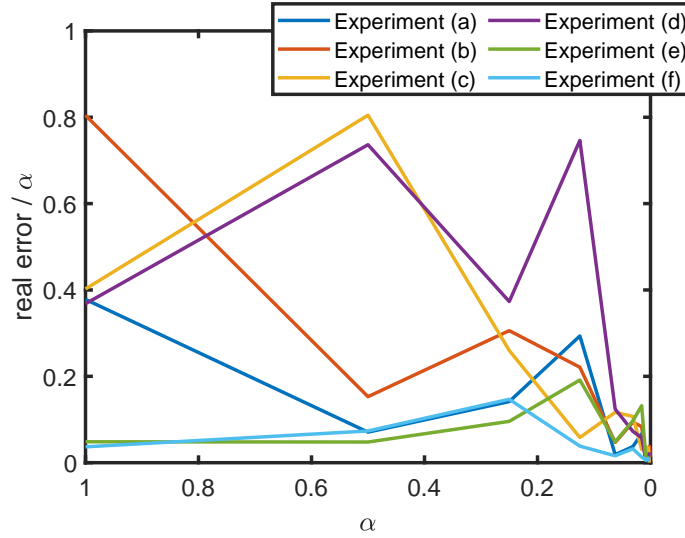

Figure 2: **Real errors versus different αs for experiments in Fig. 5.** We rerun each experiment with different user-provided αs ranging from 0 to 1. When the algorithm terminates, we compare each scattering matrix with the corresponding ground truth scattering matrix (running at a large number of sections $N = 1024$) to get the *real error* (max norm of the difference between two matrices). It shows the real error of the scattering matrix is always bounded by α. See **Data File 14** for underlying values.

References

[1] ISERLES, A. On the method of neumann series for highly oscillatory equations. *Bit Numerical Mathematics 44*, 3 (2004), 473–488.